



Biosynthesized zinc oxide using *Lycopersicon esculentum* peel extract for methylene blue degradation

C. A. Soto-Robles¹ · O. J. Nava¹ · A. R. Vilchis-Nestor² · A. Castro-Beltrán³ · C. M. Gómez-Gutiérrez¹ · E. Lugo-Medina⁴ · A. Olivas⁵ · P. A. Luque¹

Received: 8 September 2017 / Accepted: 20 November 2017 / Published online: 22 November 2017
© Springer Science+Business Media, LLC, part of Springer Nature 2017

Abstract

This work presents a study on the effects of different peel extract weight percentages in the biosynthesis of zinc oxide (ZnO) for its application in the photocatalysis. Zinc nitrate was used as a source of the zinc ions, while *Lycopersicon esculentum* (tomato) contributed the peels for the extracts to be used as a reductant and stabilizing agent. The synthesized samples were studied and characterized through Fourier transform infrared spectroscopy, X-ray diffraction, scanning electron microscopy, high resolution transmission electron microscopy and UV–Vis spectroscopy. The morphology of the surface of the material showed that samples vary in size and shape distribution depending on the amount of extract used. The band gap values were of 3.08, 3.1 and 3.18 eV for the 1, 2 and 4% concentrations, respectively. The photocatalytic properties of the ZnO were evaluated through methylene blue degradation and the results presented a 97% dye degradation in 150 min, which is more efficient than comparable commercial ZnO.

1 Introduction

An increase in the production of harmful colorants in wastewater [1, 2] has recently brought forth a need for newer, more efficient treatments designed to reduce pollutant concentration. Photocatalysis has been intensively studied due to its simplicity, low toxicity, good chemical stability, and high degradation efficiency [3]. Photocatalytic activity of this type of material has been correlated with bandgap, crystal structure, surface area, and particle size [4]. ZnO is considered one of the best photocatalysts for the degradation of organic pollutants due its high

photosensitivity, low cost, and non-toxic nature [5]. It is also one of the most exploited n-type semiconducting metal oxide materials, due to its characteristic wide direct band gap of 3.37 eV and excitation energy of 60 meV [6]. There are several methods available for the synthesis of ZnO nanoparticles such as evaporation [7], solvothermal methods [8], precipitation, electrodeposition [9], hydrothermal [10] and sol–gel [11], to name a few, these methods, however, involve long and tedious processes that also generate toxic waste. Recently, biological synthesis methods have demonstrated to be more advantageous over chemical and physical methods as they are more cost efficient and eco-friendly [12]. Biosynthesis has been applied in the synthesis of inorganic nanoparticles using biological materials, such as microorganisms, marine organisms, and plant extracts, as stabilizers and reductant agents to control the crystalline growth, favoring production of specific desired materials [13]. Some authors have developed ZnO with plant extracts and biological materials for photocatalytic activities; *Cassia fistula* [14], *Nephelium lappaceum* L. [15], *Camellia sinensis* [16], *Euphorbia prolifera* [17], *Plectranthus amboinicus* [18], *Poncirus trifoliata* [19], *Corymbia citriodora* [20], *Calotropis procera* [21]. To our knowledge, studies on the effects of using different *Lycopersicon esculentum* (tomato) peel extract concentrations on the growth of ZnO for its use in the degradation

✉ P. A. Luque
pluque@uabc.edu.mx

¹ Facultad de Ingeniería, Arquitectura y Diseño-Universidad Autónoma de Baja California, C.P. 22860, Ensenada, B.C., Mexico

² Centro Conjunto de Investigación en Química Sustentable, UAEM-UNAM, Toluca, Mexico

³ Facultad de Ingeniería Mochis, UAS, C.P. 81223, Los Mochis, Sinaloa, Mexico

⁴ Departamento de Ingeniería Química, IT de Los Mochis, Los Mochis, Sinaloa, Mexico

⁵ Centro de Nanociencias y Nanotecnología, UNAM, C.P. 22860, Ensenada, B.C., Mexico

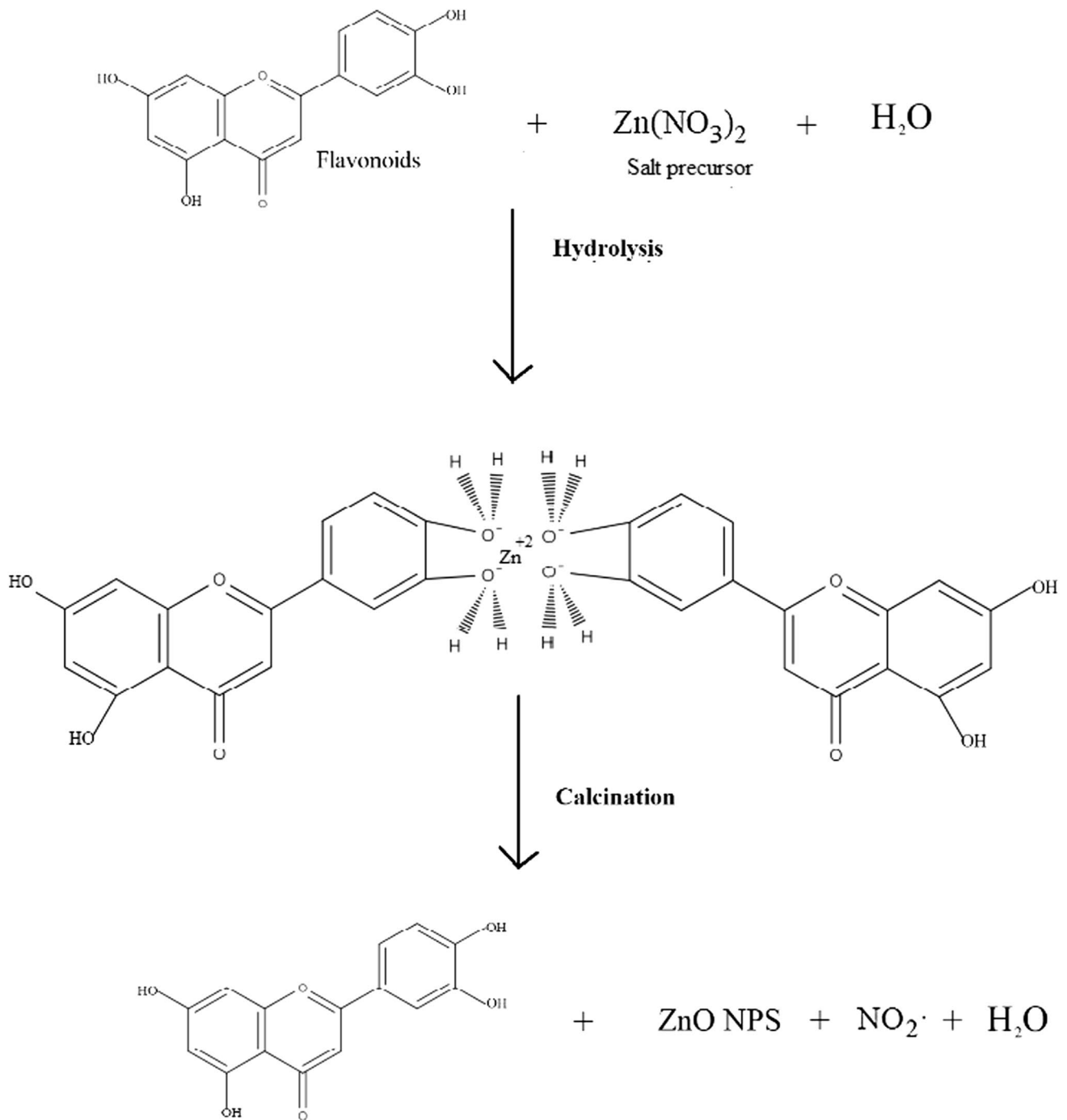


Fig. 1 Reaction mechanism for the formation of ZnO nanoparticles with *Lycopersicon esculentum* peel extract

of methylene blue (MB) have not yet been reported. In this work, we study the biosynthesis of ZnO, made while varying the *L. esculentum* extract concentrations, for evaluation in the photocatalytic degradation of methylene blue.

2 Experimental

2.1 Materials

The materials used were: the peels of *L. esculentum* (tomato); zinc nitrate ($\text{Zn}(\text{NO}_3)_2 \cdot 6\text{H}_2\text{O}$), purchased from Sigma-Aldrich; and de-ionized water as extract and synthesis medium.

2.2 Preparation of peel extracts

To start the extraction process, the tomatoes were peeled as thinly as possible and the peels were then placed in a food drier until completely dry. The dried peels were ground into a fine powder and macerated in three different mixtures at 1, 2 and 4% by weight using de-ionized water for 3 h in agitation. The mixtures were placed in sous-vide at 90 °C for 1 h. The resulting slurries were then filtered and stored in inert atmosphere glass containers for later use.

2.3 Synthesis of ZnO nanoparticles

The ZnO synthesis procedure starts with 2 g of zinc nitrate with the extract (1, 2 and 4% by weight of peels of *L. esculentum*), to make three different samples (M1, M2, and M3, respectively). The mixtures were stirred for 60 min then placed in sous-vide at 60 °C until each mixture presented a glassy caramel consistency. The mixtures were then calcinated at 400 °C for 1 h. The resulting samples were ground down into fine white powders and individually stored.

2.4 Photocatalytic activity

To study the photocatalytic activity of the resulting samples, containers with 200 mL of methylene blue (MB) at a concentration of 15 mg/L were prepared. The containers were left stirring for 30 min then exposed to a 10 W UV light bulb at 18 mJ/cm². At that point, samples of 2 mL were taken every 30 min for 2.5 h. The MB concentration was determined by measuring the absorption intensity through UV–vis spectroscopy.

2.5 Characterization

The samples were characterized via: Fourier transform infrared (FTIR), to study the chemical state; X-ray diffraction (XRD), to analyze the crystalline structure; scanning electron microscopy (SEM); and high-resolution transmission electron microscopy (HRTEM), for the study of the morphology of the samples; and ultraviolet–visible (UV–Vis) spectroscopy was used to analyze the photocatalytic activity.

3 Results and discussion

3.1 Possible reaction mechanism of ZnO nanoparticles

The reaction mechanism in the biosynthesis of ZnO is shown in Fig. 1, where the interactions between the nutritional and the functional components of the tomato can be observed;

among these are carotenoids, ascorbic acid (vitamin C), vitamin E, folic acid, flavonoids and potassium [22]. The flavonoid compounds in particular are found in both fresh and processed tomatoes, with 98% of them being specifically found in the skin (peel) of the tomato [23].

3.2 FTIR

Figure 2 shows the FTIR spectra of the synthesised ZnO NPs with different percentages (1, 2 and 4%) of the *L. esculentum* peel extract. The bands are observed at 1381 and 1632 cm⁻¹ are in the transmittance ranges of different organic molecular vibrations, present due to the organic compounds in the *L.*

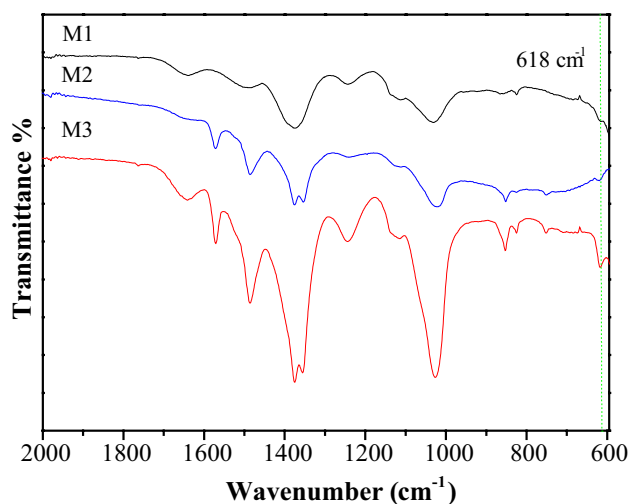


Fig. 2 FTIR spectra of the ZnO samples

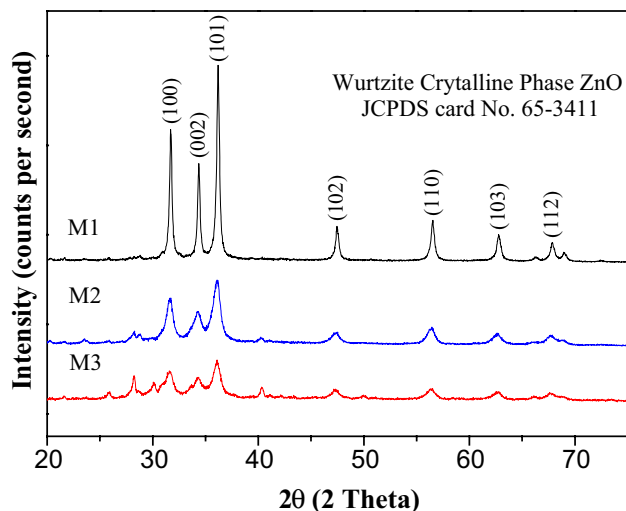


Fig. 3 XRD pattern of the ZnO samples

esculentum extract [24, 25], remainders after the synthesis process. The spectra from all the samples showed a band at 618 cm^{-1} which is characteristic of the Zn–O bond, confirming the nature of the resulting material [26].

3.3 XRD and structural study

The analysis of the XRD patterns in Fig. 3 present diffraction peaks for all samples at 31.64, 34.31, 36.23, 47.44, 56.58,

62.79 and 67.85, indexed to the (100), (002), (101), (102), (110), (103) and (112) crystal planes respectively which belong to the wurtzite crystalline phase (PDF # 65-3411, Hexagonal) of ZnO [27]. A few unassigned peaks were also noticed in the vicinity of the characteristic peaks. These sharp Bragg peaks might be due to the organic content in the higher extract weight percentages acting as capping agents in the synthesis reaction [28]. Scherrer's formula, that is $\tau = K\lambda/\beta\cos\theta$, was used to calculate the average crystal size of each sample, where: τ , the mean size of the crystalline

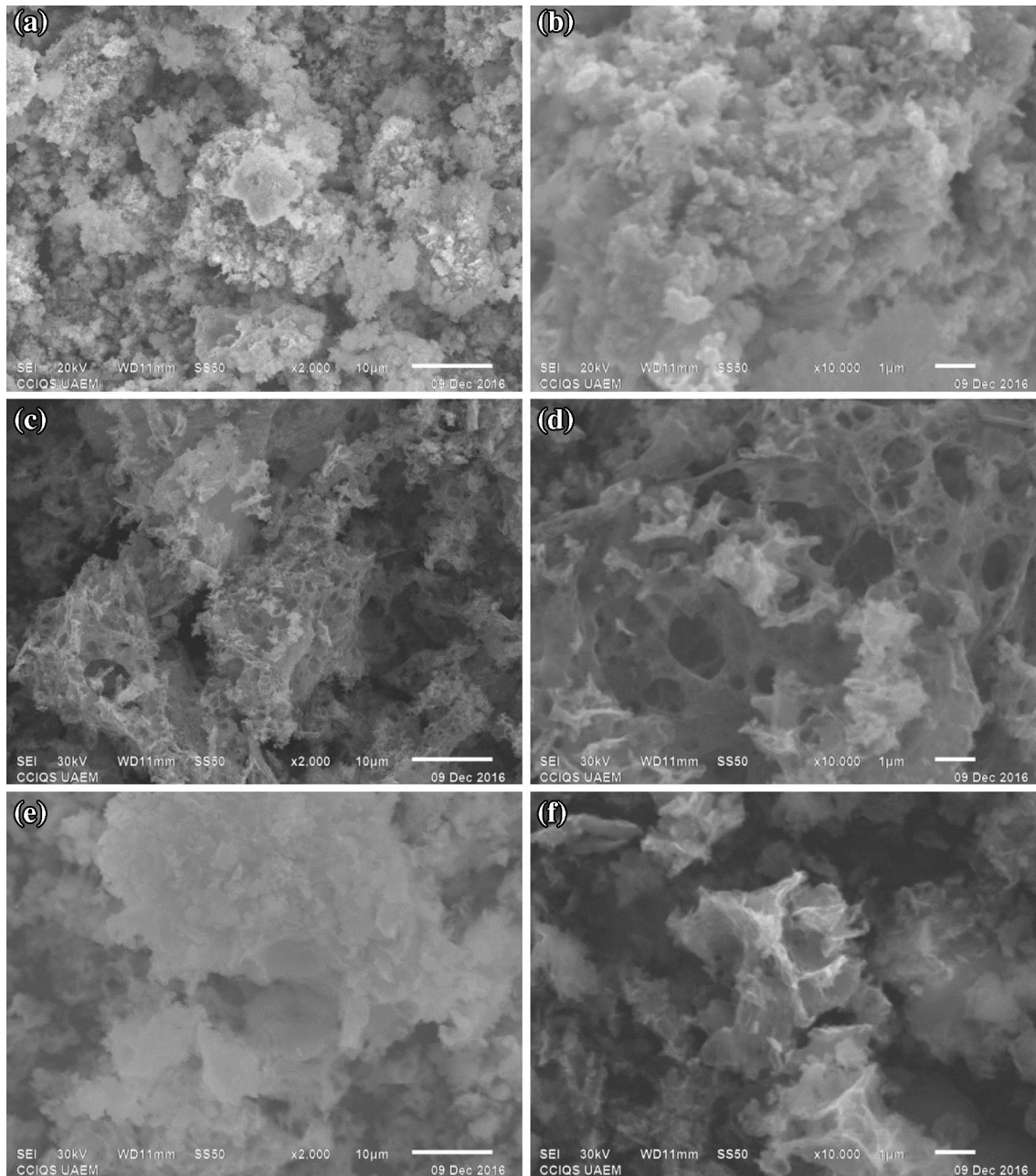


Fig. 4 SEM micrographs of ZnO acquired at $\times 2000$ and $\times 10,000$ for M1 (a, b), M2 (c, d), and M3 (e, f) samples, respectively

domains; K , a dimensionless value of 0.9; λ , X-ray wavelength; β , full width at half maximum intensity; and θ , the Bragg angle [29]. The sizes of the crystals calculated from the XRD spectra were 20, 12 and 7 nm for M1, M2 and M3, respectively.

3.4 Morphological study

The SEM micrographs in Fig. 4 show the effects of the different extract concentrations on the surface morphology of the ZnO material. Here, the difference made by the extract

can be appreciated as the material changes when more extract is used; from agglomerates in Fig. 4a, to largely porous structures in Fig. 4b, c that shows structures where pores superimpose each other, creating a web like structure, which in turn could give the material a higher surface area. In accordance with the SEM results, the transmission electron microscopy micrographs, shown in Fig. 5, show that the samples with a weight percentage of 1% had an average size of (M1) 6.54 ± 4.5 nm, as seen in histogram a of Fig. 5c, and an undefined morphology. At higher percentages by weight of the tomato peel extract

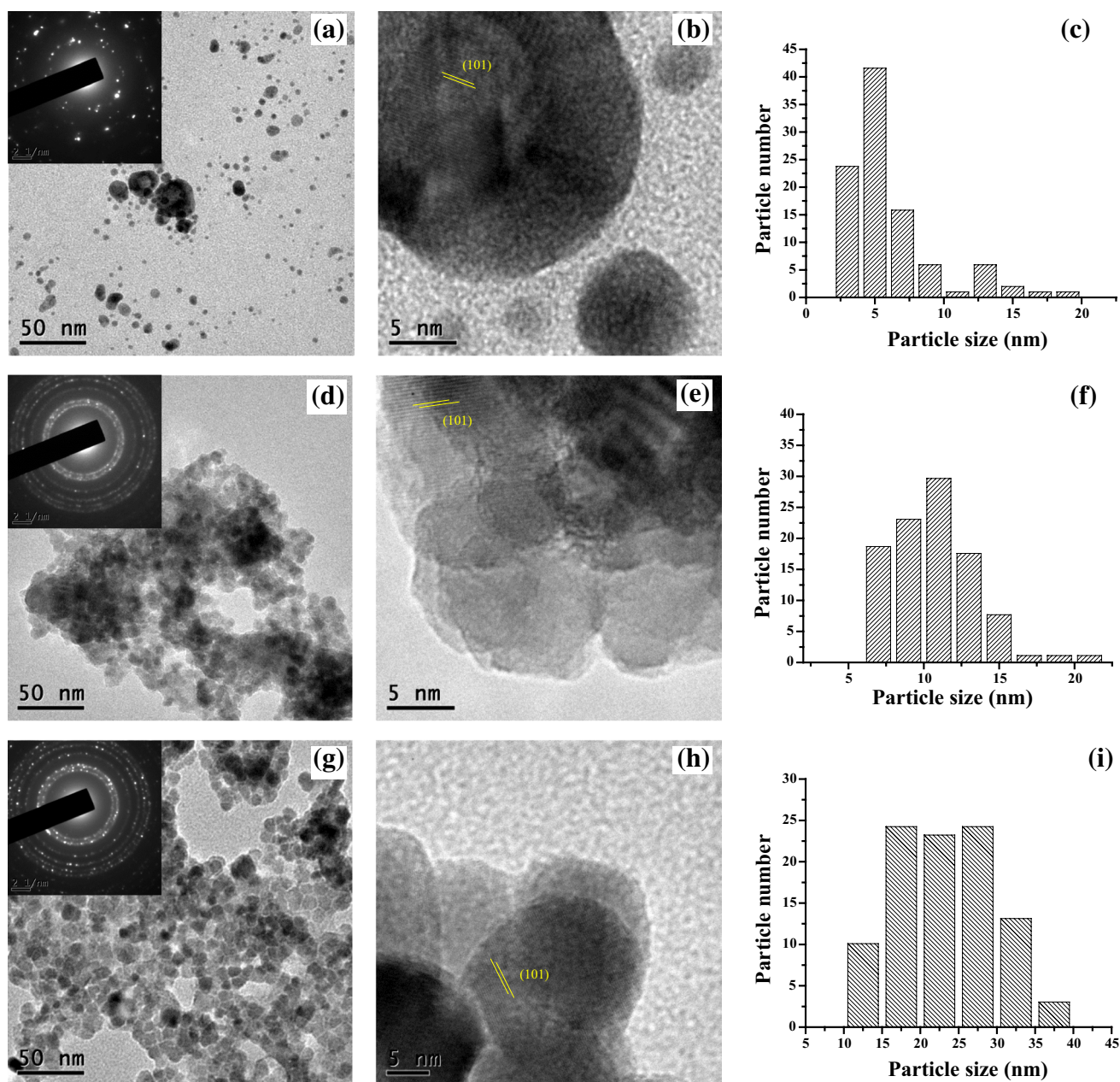


Fig. 5 Analysis of ZnO NPs, where **a–c** M1, **d–f** M2 and **g–i** M3. Insets show electron diffraction pattern of **a**, **d** and **g**, respectively

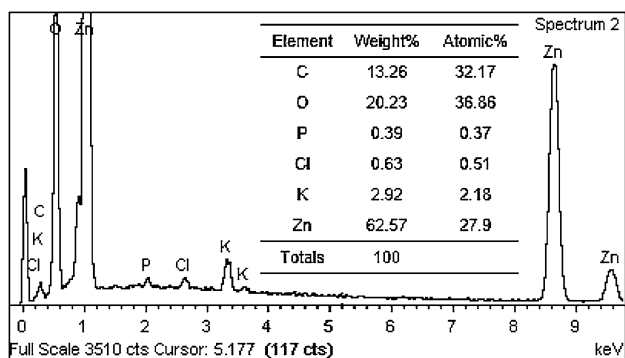


Fig. 6 Energy dispersive spectra of the ZnO nanoparticles

used during the biosynthesis, the samples presented a better distribution of size and a more homogeneous growth of its particles, which generated a better morphological control, as seen in Fig. 5f, as well as an increase in the

average size of the ZnO crystals with a narrower standard deviation (10.75 ± 2.9 nm), that is to say a better size distribution. Lastly, although the sample with a weight percentage of 4% (M3), observed in Fig. 5i, presented particles with a larger average size ($> 24 \pm 7.9$ nm), it also presented the best morphological control by means of the size distribution of the synthesized particles. This means that the sizes of the particles in sample M3 were closer to the average size for that sample when compared to the particles in samples M1 and M2 and their respective average particle sizes. The HRTEM micrographs in Fig. 5b, e, h clearly show lattice lines (101), for the three samples with an interplanar space of 2.4 Å, indicating the hexagonal structure of the ZnO particles. The Insets in Fig. 5a, d and g show the selective area electron diffraction patterns (SAED), which reveal diffraction rings corresponding to reflections (101), (100), and (002), which can be related to the hexagonal crystal structure of the zinc oxide. The diffraction rings are associated with the polycrystalline

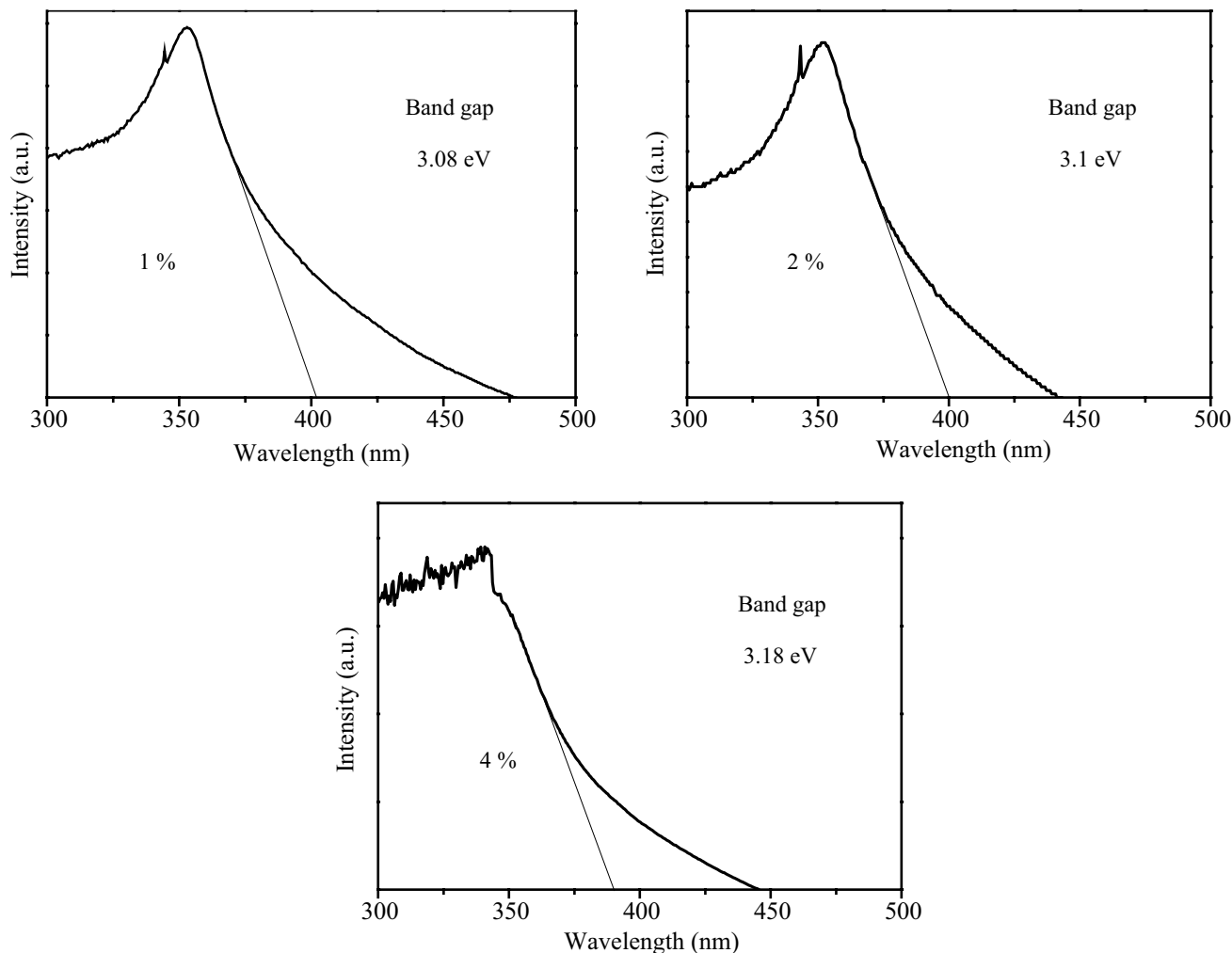


Fig. 7 Absorption spectrum of the ZnO nanoparticles with different percentages 1, 2 and 4% of the *Lycopersicon esculentum*

nature of the three different samples, and are in agreement with the X-ray diffraction signals, indexed on the basis of the wurtzite crystal structure of zinc oxide (pdf # 65-3411).

3.5 Energy dispersive spectra of ZnO nanoparticles

In Fig. 6, the results of the study of the elemental composition by means of EDS are observed. All three samples showed a similar composition, and only a small increase in the amount of the potassium ions was observed with the increase in the weight percentage of the peel extract. Additionally, the presence of ZnO and other elements commonly found in tomato peel extract were corroborated [30].

3.6 UV–Vis diffuse reflectance spectra of ZnO nanoparticles

The materials synthesized with *L. esculentum* were analyzed through UV–Vis to determine the band gap, as shown in Fig. 7. The materials exhibited absorption at the 395, 390 and 400 nm wavelengths. The determination of the values of each material was made by means of the $E_g = hc/outset$ equation, where E_g is the band gap, h is the Planck constant, c is the speed of light ($hc = 1240 \text{ eV nm}$) and outset is the value in which the wavelength intersects the X-axis [31]. The band gap values presented by the synthesized materials were 3.08, 3.1 and 3.18 eV for the concentrations of 1, 2 and 4% of the extract, respectively. These values are similar to those previously reported for ZnO nanoparticles [32]. The small changes in the energy gap are associated with the size of the nanoparticles; the smaller the particle, the greater the band gap. As the change in the percentage of mass in the biosynthesis of the materials had an effect on the size of the nanoparticles, as in the greater the W%, the smaller the size, this indirectly affected the values of the band gap. In addition to the particle size, these band gap values may also vary due to the presence of K ions in the ZnO samples; affecting the interactions of the electrons between the conduction band and the valence band. Here, a co-relation between the band gap energy and the K ion content was observed, that is, the band gap values increased as did the concentration of K ions in the sample [33].

3.7 Catalytic activity

Figure 8 shows the MB degradation photocatalytic under UV irradiation and degradation rate constants (K) of the biosynthesized ZnO nanoparticles. As shown in Fig. 8a, sample M1 exhibits a degradation of around 45% at 90 min, while, the other samples show a higher

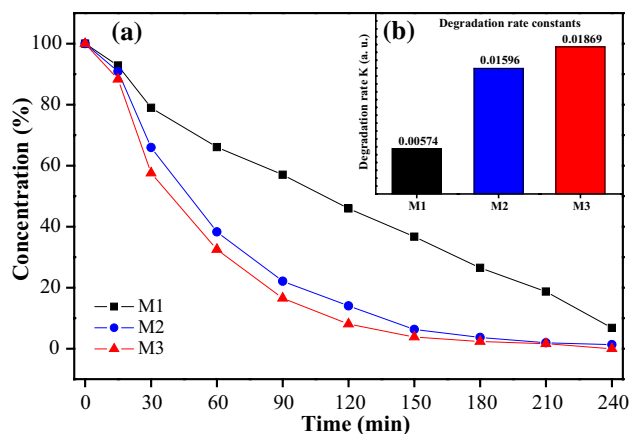


Fig. 8 Photocatalytic activity (a) and degradation rate constants (b) of the ZnO materials

photocatalytic activity at around 78 and 85% at 90 min for M2 and M3, respectively. Figure 8b shows the degradation rate constants (K) values at around 0.0057, 0.0160 and 0.0187 for M1, M2 and M3, respectively. With all of this, we can appreciate that the ZnO material of sample M3, made with a *L. esculentum* extract concentration at 4% by weight, has both a better degradation performance and a higher K when compared with the other samples, possibly due to the better size distribution of the particles [34], resulting in a higher performance, more noticeable yet when compared to chemically synthesized commercial NPs that only display a 37% degradation at 120 min [35].

4 Conclusions

This work shows a green approach to the synthesis of ZnO through green chemistry via the use of different *L. esculentum* extract amounts. The crystalline size and homogeneity of the resulting material seems to be influenced by the amount of extract used during the synthesis. The photocatalytic activity for the sample with 4% extract by weight presented a MB degradation of 92% at 120 min, which is an improvement when compared to similar commercially available material.

Acknowledgements The authors acknowledge the support of the Universidad Autónoma de Baja California through the 492 project. We thank to Nayely Torres from CCIQS for microscopy technical support.

References

1. T. Robinson, G. McMullan, R. Marchant, P. Nigam, *Bioresour. Technol.* **77**, 247 (2001)

2. Y.Z. Chen, N. Li, Y. Zhang, L.D. Zhang, J. Colloid Interface Sci. **422**, 9 (2014)
3. D. Sudha, P. Sivakumar, Chem. Eng. Prog. **97**, 112 (2015)
4. A. Ashar, M. Iqbal, I.A. Bhatti, M.Z. Ahmad, K. Qureshi, J. Nisar, I.H. Bukhari, J. Alloys Compd. **678**, 126 (2016)
5. P. Mishra, Y.P. Singh, H.P. Nagaswarupa, S.C. Sharma, Y.S. Vidya, S.C. Prashantha, L. Renuka, J. Alloys Compd. **685**, 656 (2016)
6. F.T. Thema, E. Manikandan, M.S. Dhlamini, M. Maaza, Mater. Lett. **16**, 124 (2015)
7. B.D. Yao, Y.F. Chan, N. Wang, Appl. Phys. Lett. **81**, 757 (2002)
8. L. Xu, Y.L. Hu, C. Pelligra, C.H. Chen, L. Jin, H. Huang, S.L. Suib, Chem. Mater. **21**, 2875 (2009)
9. E.M. Elsayed, A.E. Shalan, M.M. Rashad, J. Mater. Sci. Mater. Electron. **25**, 3412 (2014)
10. N. Ekthammathat, S. Thongtem, T. Thongtem, A. Phuruangrat, Powder Technol. **254**, 199 (2014)
11. T. Ates, C. Tatar, F. Yakuphanoglu, Sens. Actuators A **190**, 153 (2013)
12. K. Elumalai, S. Velmurugan, Appl. Surf. Sci. **345**, 329 (2015)
13. S. Azizi, F. Namvar, R. Mohamad, P.M. Tahir, M. Mahdavi, Mater. Lett. **148**, 106 (2015)
14. D. Suresh, P.C. Nethravathi, H. Rajanaika, H. Nagabhushana, S.C. Sharma, Mater. Sci. Semicond. Process. **31**, 446 (2015)
15. T. Karnan, S.A.S. Selvakumar, J. Mol. Struct. **1125**, 358 (2016)
16. O.J. Nava, P.A. Luque, C.M. Gomez-Gutierrez, A.R. Vilchis-Nestor, A. Castro-Beltran, M.L. Mota-Gonzalez, A. Olivias, J. Mol. Struct. **1134**, 121 (2017)
17. S.S. Momeni, M. Nasrollahzadeh, A. Rustaiyan, J. Colloid Interface Sci. **472**, 173 (2016)
18. L. Fu, Z. Fu, Ceram. Int. **41**, 2492 (2015)
19. P.C. Nagajyothi, T.M. An, T.V.M. Sreekanth, J.I. Lee, D.J. Lee, K.D. Lee, Mater. Lett. **108**, 160 (2013)
20. Y. Zheng, L. Fu, F. Han, A. Wang, W. Cai, J. Yu, F. Peng, Green Chem. Lett. Rev. **8**, 59 (2015)
21. V.V. Gawade, N.L. Gavade, H.M. Shinde, S.B. Babar, A.N. Kadam, K.M. Garadkar, J. Mater. Sci. Mater. Electron. **1**, 1 (2017)
22. W. Klunklin, G. Savage, Foods **6**, 56 (2017)
23. R.K. Toor, C.E. Lister, G.P. Savage, Int. J. Food Sci. Nutr. **56**, 597 (2005)
24. S. Vermeir, K. Beullens, P. Mészáros, E. Polshin, B.M. Nicolai, J. Lammertyn, Sens. Actuators B **137**, 715 (2009)
25. Y. Lu, J.D. Miller, J. Colloid Interface Sci. **256**, 41 (2002)
26. R. Yuvakkumar, J. Suresh, B. Saravanakumar, A.J. Nathanael, S.I. Hong, V. Rajendran, Spectrochim. Acta A **137**, 250 (2015)
27. Y. Chen, L. Zhang, L. Ning, C. Zhang, H. Zhao, B. Liu, H. Yang, Chem. Eng. **264**, 557 (2015)
28. T.C. Prathna, N. Chandrasekaran, A.M. Raichur, A. Mukherjee, Colloids Surf. B **82**, 152 (2011)
29. X. Zhang, Y. Chen, S. Zhang, C. Qiu, Sep. Purif. Technol. **172**, 236 (2017)
30. G. Beecher, Proc. Soc. Exp. Biol. Med. **218**, 98 (1998)
31. G.V. Khade, M.B. Suwarnkar, N.L. Gavade, K.M. Garadkar, J. Mater. Sci. Mater. Electron. **26**, 3309 (2015)
32. N. Kamarulzaman, M.F. Kasim, R. Rusdi, Nanoscale Res. Lett. **10**, 346 (2015)
33. M. Stan, A. Popa, D. Toloman, A. Dehelean, I. Lung, G. Katona, Mater. Sci. Semicond. Process. **39**, 23 (2015)
34. K. Koci, L. Obalova, L. Matejova, D. Placha, Z. Lacny, J. Jirkovsky, O. Solcova, Appl. Catal. B **89**, 494 (2009)
35. M. Azarang, A. Shuhaimi, R. Yousefi, S.P. Jahromi, RSC Adv. **5**, 21888 (2015)